Open Archive TOULOUSE Archive Ouverte (OATAO)

OATAO is an open access repository that collects the work of Toulouse researchers and makes it freely available over the web where possible.

Any correspondance concerning this service should be sent to the repository administrator: staff-oatao@inp-toulouse.fr.

Structural and electrical properties of gold nanowires/P(VDF-TrFE) nanocomposites

Antoine Lonjon[1]**, Lydia Laffont**[2]**, Philippe Demont**[1]**, Eric Dantras**[1] **and Colette Lacabanne**[1]

[1] Laboratoire de Physique des Polymères, CIRIMAT/Institut Carnot, Université Paul Sabatier, 118 route de Narbonne, 31062 Toulouse cedex 9, France

[2] CIRIMAT/Institut Carnot, ENSIACET, 4 allée Emile Monso, 31432 Toulouse Cedex 4, France

E-mail: demont@cict.fr

Abstract

High aspect ratio gold nanowires were uniformly dispersed into a poly(vinylidene difluoride–trifluoroethylene) [P(VDF-TrFE)] matrix. The nanowires were synthesized by electrodeposition using nanoporous anodic alumina oxide templates. The intrinsic optical conductivity of the gold nanowires was determined by valence electron energy loss spectroscopy. The effect of increasing volume fraction of Au nanowires on the morphology and crystallization of P(VDF-TrFE) matrix was investigated by differential scanning calorimetry. The crystallinity of P(VDF-TrFE) is strongly depressed by the randomly dispersed nanowires. Above 30 vol% the crystallization of P(VDF-TrFE) is suppressed. The bulk electrical conductivity of nanocomposite films, at room temperature, obeys a percolation behaviour at a low threshold of 2.2 vol% and this was confirmed using the surface resistivity value. An electrical conductivity of $100\,\mathrm{S\,m^{-1}}$ is achieved for a 3 vol% filler content.

1. Introduction

Polymer composites reinforced with a low content of strong fillers can significantly improve the mechanical, thermal and electrical properties of the pure polymer matrix. Moreover, these improvements are achieved through conventional processing techniques without any detrimental effects on the processability of the matrix. Typical mixed fillers used in polymer matrices are carbon black [1–3], carbon nanotubes (CNTs) [4, 5] and metal nanoparticles [6, 7]. These studies showed that electrical and mechanical properties of reinforced polymer composites depend on many factors, such as inherent properties, degree of dispersion, orientation [8], interfacial adhesion, aspect ratio and content of filler. The degree of dispersion is, in particular, well known as one of the most important factors in electrical properties and is difficult to control in nanocomposites. Experimentally observed percolation threshold was known to be strongly dependent on the aspect ratio of the filler and not on their nanometric size. Very low percolation threshold was obtained with

aspect ratios ζ (ratio of length to width) higher than 100 and even 1000. Metal nanowires (NWs) have attracted considerable attention because of their specific properties such as electrical conductivity [9] and magnetic susceptibility [10–12]. Nickel nanowires (Ni NWs) have a high surface reactivity due to the nanometric dimension. This reactivity of Ni NW induces surface oxidation. To elaborate conductive nanocomposites, the Ni NWs required the removal of the oxide layer on their surface prior to their introduction into a poly(vinylidene difluoride–trifluoroethylene) [P(VDF-TrFE)] copolymer matrix in order to reach high conductivity at a low filler content [13]. P(VDF-TrFE) is a semi-crystalline thermoplastic polymer with excellent processability, high mechanical strength, high dielectric permittivity and thermal stability. But its degree of crystallinity was affected by filling it with nanoparticles such as carbon nanofibre (CF) [14], CNTs [15] or nanoclays [16, 17]. The mechanical properties are directly linked to the crystallinity ratio.

In this study, gold nanowires (Au NWs) were prepared in order to elaborate high conductive nanocomposites at

low Au NW volume fractions to preserve the mechanical properties of the P(VDF-TrFE) matrix. The optical conductivity of the Au NWs was extracted from valence electron energy loss spectroscopy (VEELS) spectra in combination with transmission electron microscopy (TEM). The influence of Au NWs' content and their aspect ratio on the crystallization of P(VDF-TrFE) and on the electrical properties of Au NW/P(VDF-TrFE) nanocomposites was investigated. Structural analysis and physical performances of the resulting nanocomposite materials were examined using scanning electron microscopy (SEM), differential scanning calorimetry (DSC) and dc and ac conductivity measurements. The influence of preparation and processing conditions on the percolation threshold was discussed.

2. Experimental section

2.1. Materials and sample preparation

2.1.1. Au NW synthesis. Au NWs were synthesized by electrochemical deposition in an anodic aluminium oxide (AAO) porous template using a free cyanide electrolyte. Direct current (dc) electrodeposition was carried out at 50 °C using a gold wire of 1.0 mm diameter as the anode. A porous AAO membrane of 200 nm diameter and 50 μm thickness was supplied by Whatman. One side of the AAO membrane was coated with a 35 nm thick silver layer using a sputtering technique as cathode for electrodeposition. The growth of Au NWs was controlled by the time of deposition and the direct current intensity using a Keithley 2420 source meter. The AAO membrane was dissolved in 6M NaOH for 30 min, releasing Au NWs from the template.

High purity Au NWs as fillers are of considerable interest in order to achieve high dc conductivity in nanocomposites. Filling AAO membrane pores with Au was performed using a direct current intensity of 3 mA under a voltage of 0.7 V. The morphology of the Au NWs was characterized by SEM to determine the aspect ratio ζ. The Au NWs exhibit a uniform length of 45 μm and a regular diameter of 200 nm. The silver-coated layer backside and the AAO membrane were dissolved in HNO$_3$ and NaOH solution, respectively. The NW suspension was then filtered through a polyamide (200 nm pore size) membrane. The filtered NWs were stored in acetone and dispersed using an ultrasonic bath. A droplet of this solution was deposited onto a SEM pin.

For comparison, bulk Au powder with particle size in the range 0.5–10 μm, supplied by Aldrich, was chosen.

2.1.2. Nanocomposite preparation. P(VDF-TrFE) (70/30) mol% copolymer was supplied by Piezotech S.A. (Saint Louis, France). The melting temperature was determined to be 150 °C by DSC and the density was about 1.8 g cm^{-3}.

The nanocomposites were prepared by the solvent casting method. P(VDF-TrFE) was dissolved in acetone. Nanoparticles were poured into the polymer solution and the mixture was submitted to 5 s short pulse of sonication, corresponding to a dissipated power of 25 W. A slight curvature of Au NWs is observed after sonication because of the ductility

and high aspect ratio of Au NWs. The sonication parameters were optimized by the observation of Au NWs dispersion using SEM. The solvent was evaporated using a magnetic stirrer at 80 °C for 1 h. Pellets of randomly dispersed Au NWs in P(VDF-TrFE) matrix were obtained. Films with 200 μm thickness were moulded in a hot press at 200 °C under a pressure of about 0.3 MPa. The coating samples were elaborated by spray coating. The matrix was dissolved in acetone and NWs were poured into the polymer solution. This mixed suspension was sprayed as a coating on a glass substrate of 120 mm × 120 mm. The coating is about 20 μm thick. It was heated at 80 °C for 1 h to evaporate the solvent. No residue of solvent was found in the thermogravimetric analysis, indicating the complete removal of acetone from the films and coatings.

Au NWs/P(VDF-TrFE) nanocomposites were elaborated with a volume fraction varying from 0 to 30 vol%.

2.2. Differential scanning calorimetry

Crystallization and melting of the nanocomposites were investigated using a TA Instruments 2920 differential scanning calorimeter. The temperature of the calorimeter was calibrated using the onset of melting of tin (T_m = 231.88 °C), indium (T_m = 156.6 °C) and cyclohexane (T_m = 6 °C) at a heating rate of 10 °C min^{-1}. The heat-flow rate was calibrated with the heat of fusion of indium (28.45 J g^{-1}), then refined with a baseline run of two empty Al pans and a calibration run with sapphire as a standard. Before the heating and cooling runs, the samples were melted at 200 °C and maintained at this temperature for 5 min in order to erase the thermal history. The samples were then cooled from 200 to 20 °C at a rate of 10 °C min^{-1} and then heated from 20 to 200 °C at 10 °C min^{-1}. All the DSC measurements were performed in N$_2$ atmosphere.

The transition temperatures were taken as the peak maximum or minimum in the DSC curves. The degree of crystallinity of the P(VDF-TrFE) composites was calculated according to the following equation: $\chi_c = \Delta H_m / (\Delta H^0_{m,P(VDF-TrFE)}) wt\%_{P(VDF-TrFE)}$ where ΔH_m and $wt\%_{P(VDF-TrFE)}$ are, respectively, the apparent melting enthalpy and the weight fraction of P(VDF-TrFE) in the composites and $\Delta H^0_{m,P(VDF-TrFE)}$ the value of enthalpy corresponding to a 100% crystalline P(VDF-TrFE) (70/30) copolymer, taken as 91.45 J g^{-1} [18].

2.3. Optical conductivity of Au NWs

The intrinsic optical conductivity of the Au NWs was studied using VEELS. VEELS experiments were carried out using a high resolution Gatan imaging filtering (HRGIF) system in a Tecnai F20 transmission electron microscope equipped with a Wien-filter type monochromator at the National Centre for High Resolution Electron Microscopy (HREM) of Delft University of Technology. A 100 kV operation voltage allowed an energy resolution of 0.50 eV as determined from the full width at half maximum of the zero-loss peak. The VEELS spectra were collected with an energy dispersion of 0.1 eV/channel, an illumination semi-angle α

of 2.5 mrad and a collection semi-angle β of 6.5 mrad. The dielectric function was calculated using the 'Epsilon' software performing deconvolution, angular correction, normalization and Kramers–Krönig (KK) transformation successively [19]. Prior to any quantitative analysis of the VEELS data, the spectrum was corrected for the point-spread function (PSF) of the instrumentation by a Fourier-ratio deconvolution followed by a Fourier-log deconvolution to eliminate contributions from plural scattering. The material loss function $Im(-1/\varepsilon(E))$ is extracted after angular correction and normalization of the signal. The real part $Re(1/\varepsilon)$ is calculated using a KK transformation. $Re(\varepsilon)$ and $Im(\varepsilon)$ are then deduced. So the optical conductivity $\sigma(E)$ can be deduced [20, 21] using the following relation implanted in the Epsilon software [19]:

$$\sigma(E) = \frac{E \, Re(\varepsilon) Im(\varepsilon)}{\hbar}. \tag{1}$$

2.4. Electrical conductivity

The bulk electrical conductivity of the nanocomposites was measured by recording the complex conductivity $\sigma^*(\omega)$ using a Novocontrol broadband spectrometer. The measurements were carried out in the frequency range from 10^{-2} to 10^6 Hz at room temperature. The real part $\sigma'(\omega)$ of the complex conductivity $\sigma^*(\omega)$ was investigated. For all the nanocomposite samples considered in this study, the phase lag between the measured impedance and the applied ac voltage was negligible at low frequencies, so that the reported impedance at 0.01 Hz is equivalent to the dc resistance. The dc conductivity σ_{dc} of the samples was determined from the independent frequency part of $\sigma'(\omega)$ [4], i.e. the low frequency plateau. Films of 200 μm thickness were introduced between two circular gold plated electrodes (20 mm in diameter). To reduce contact resistivity with the cell electrodes, a thin layer of gold (100 nm) was sputtered onto both sides of the films using a BOC Edwards Scancoat Six Sputter Coater.

The surface resistivity ρ_s of the nanocomposite films was studied using a concentric ring-probe technique. Surface resistance R_s was measured using a Keithley 2420 source meter in a four-probe configuration and converted to surface resistivity.

3. Results and discussion

The Au NWs, released from the membrane, are well dispersed in the acetone suspension, as shown in the SEM image in figure 1. The EDX spectrum was recorded to prove the chemical nature of the Au NWs. The Au peak has the most prominent intensity indicating that the NWs are made up of metallic gold. The weak peaks at low energies reveal the presence of oxygen and aluminium coming from the AOO template. The Au NWs occur individually, no bundles and no sonication-induced damage are observed except for a slight curvature. Figure 2 shows the SEM image of a matrix filled by 7.7 vol% of Au NWs. As in the acetone suspension, Au NWs occur individually in the P(VDF-TrFE) matrix. The SEM image shows a slight orientation of the NWs
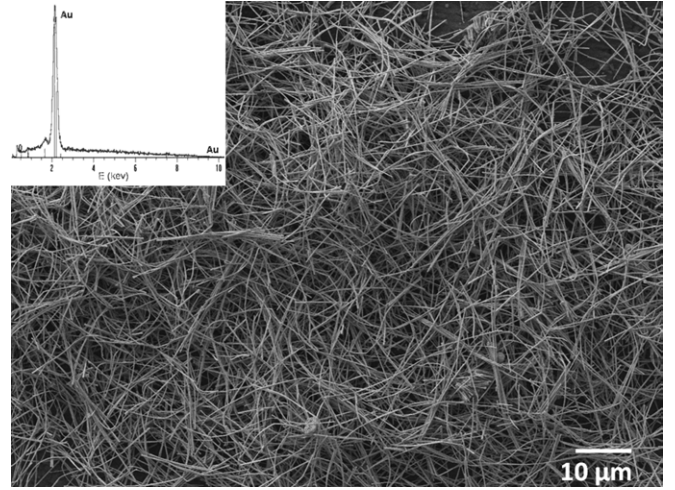

Figure 1. SEM image and EDX spectrum of Au NWs after complete removal of AAO membrane and dispersion in acetone.
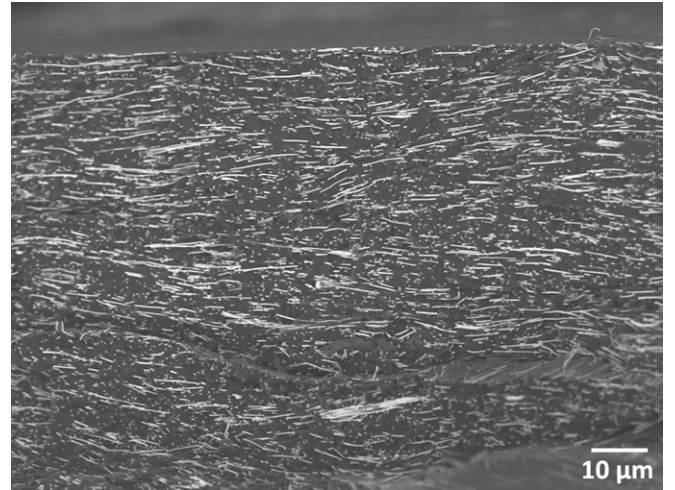

Figure 2. SEM image of the cryofractured surface of Au NW/P(VDF-TrFE) nanocomposites with 7.7 vol% Au content.

resulting from the compression moulding processing of the nanocomposites.

3.1. Intrinsic conductivity of a single Au NW

High angle annular dark field (HAADF) image of the Au NWs associated with the VEEL spectrum is presented in figure 3. A small probe (0.5 nm) was used to acquire all the VEEL spectra for which the shape remains identical along a NW and for different NWs. The dielectric function and the optical conductivity were calculated using the 'Epsilon' software. Since the intensive zero-loss peak hides the fine structure below 1 eV, $\sigma(E)$ is significant only above 1 eV. Thus, to determine the electrical conductivity at $E = 0$ eV, the electrical conductivity is extrapolated linearly in the range between 1 and 0 eV starting from 1 eV [20]. Assuming that this extrapolation is correct, the electrical conductivity of Au NW is 72×10^6 S m^{-1}. This value is consistent with other observations for bulk (45×10^6 S m^{-1}) and with four-probe measurements on Au NWs [22].
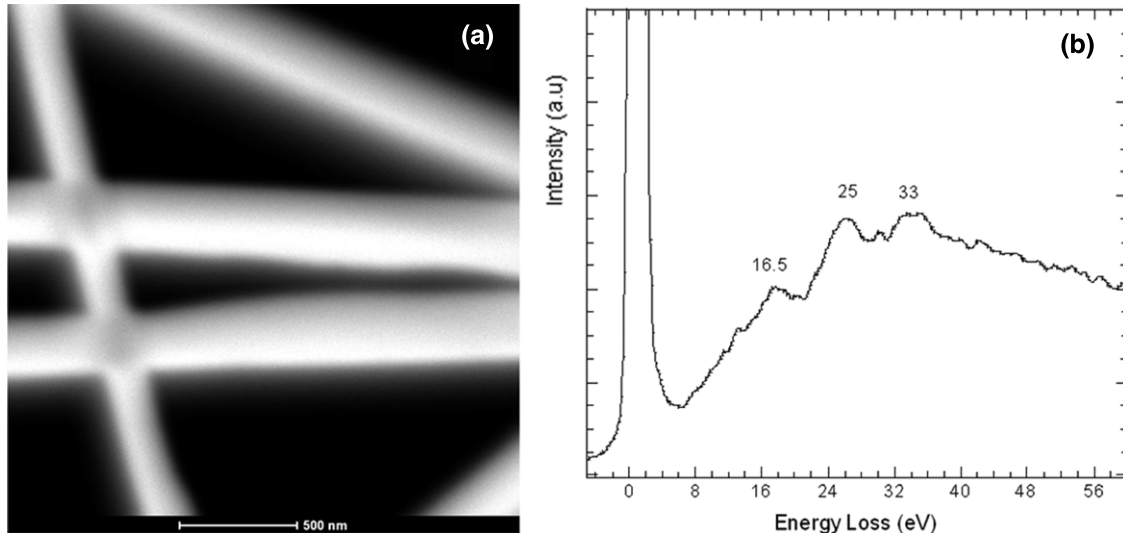
Figure 3. (*a*) HAADF image of Au NWs and (*b*) VEEL spectrum of Au NWs.
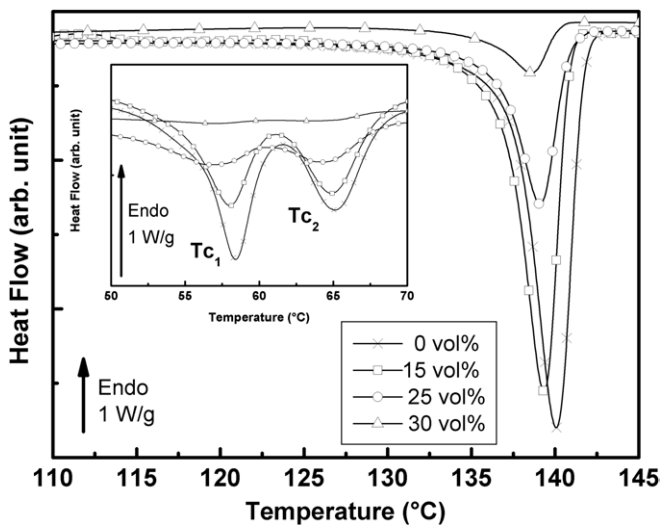

Figure 4. DSC thermograms upon cooling of P(VDF-TrFE) ($\times$) and Au NW-filled P(VDF-TrFE) nanocomposites with 15 ($\square$), 25 ($\bigcirc$) and 30 vol% ($\triangle$).

Figure 5. Degree of crystallinity χ_c of P(VDF-TrFE) matrix as a function of Au volume fraction and particle size: ($\blacksquare$) Au NWs, ($\bigcirc$) 500 nm, ($\triangle$) 10 μm. Lines correspond to the best fitting.

3.2. P(VDF-TrFE) crystallization inhibition

Figure 4 shows the DSC curves of the Au NW/P(VDF-TrFE) nanocomposites recorded during cooling scans. These curves exhibit a crystallization and para-ferroelectric (p-f) transition at 140 °C and 60 °C, respectively. These two exothermic events were used to calculate the degree of crystallinity χ_c of P(VDF-TrFE). The glass transition T_g of the matrix, generally observed around −30 °C, is ill-defined. The insert of figure 4 shows a magnification of the Curie transition temperature range. The two exothermic peaks, reported by Tanaka *et al* [23] and discussed by Moreira *et al* [24] and Gregorio and Botta [25] in terms of a mixture of two crystalline phases, are clearly observed. The low-temperature peak T_{c1} was assigned to the Curie transition in a less ordered crystalline phase. The high-temperature peak T_{c2} is attributed to well-formed crystallites. For all Au NW volume fractions, no significant change in the temperature of p-f transition and crystallization was observed.
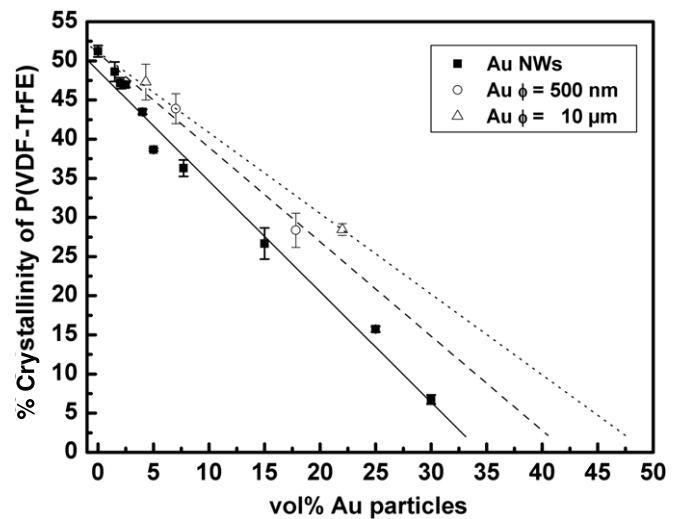
The influence of Au particles on the crystallization of P(VDF-TrFE) is illustrated in figure 5. The degree of crystallinity χ_c decreases linearly as a function of the Au volume fraction. As shown previously, the presence of the dispersed NWs induces a slight decrease in the shape and temperature of transition peaks. The crystallinity of the P(VDF-TrFE) matrix is inhibited gradually by a decrease in the number of crystallites. A linear extrapolation of the experimental points until zero crystallinity (solid line) gives a critical Au NW volume fraction of 35 vol%. The effect of a dispersion of nanoclays on the crystallinity behaviour of PVDF and its copolymer has been largely described by Cebe and Runt [16] and Dillon *et al* [17]. The presence of nanoclays induced a weak decrease in the crystallinity and a shift of the melting peak towards lower temperatures. Up to 25 wt% of nanoclays, this concomitant decrease becomes drastic [16]. Carbon fibre (CF)-filled PVDF nanocomposites exhibited a
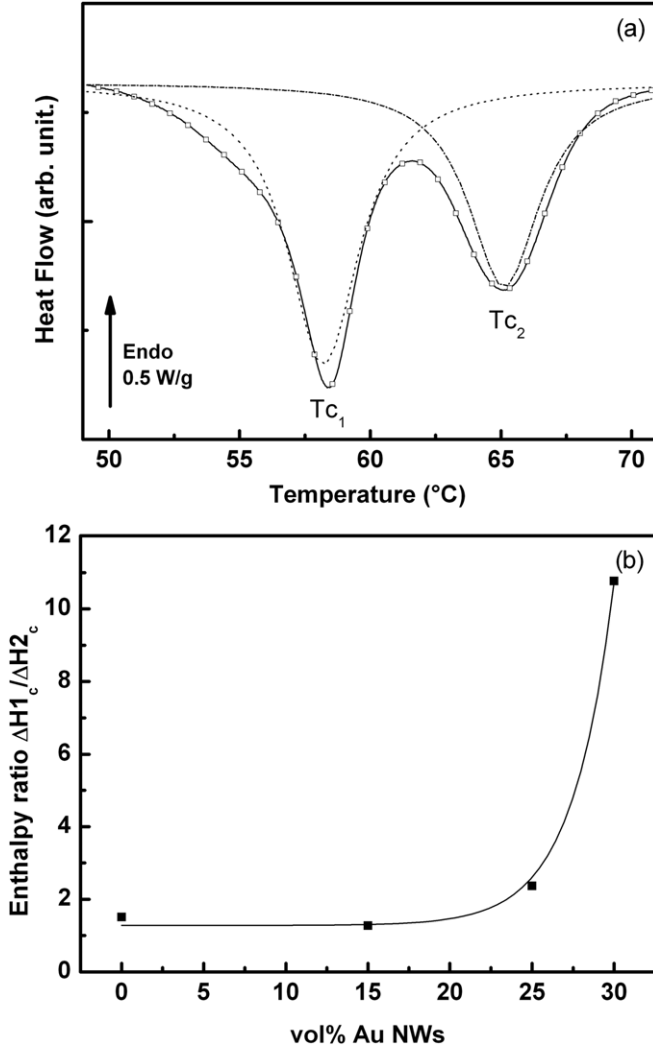
Figure 7. Dependence of the dc conductivity σ_{dc} versus Au NW volume fraction at 25 °C. The solid line connecting symbols is a guide to the eye. The inset shows the log–log plot of σ_{dc} versus $(p - p_c)$ with $p_c = 2.2$ vol% and $t = 1.21$. The solid line corresponds to the best-fitted line.

be drastically different between the two crystalline phases. A peak deconvolution procedure was used to investigate the Curie transition in terms of the coexistence of two crystalline phases. The enthalpies ΔH_{C1} and ΔH_{C2} of the deconvoluted exothermic peaks were determined and the ratio $\Delta H_{C1}/\Delta H_{C2}$ was reported as a function of Au NWs volume fraction in figure 6(*b*). Above 20 vol%, the ratio $\Delta H_{C1}/\Delta H_{C2}$ increases drastically which is characteristic of a strong modification in the P(VDF-TrFE) crystalline phase structure. Above this critical volume fraction, the low-temperature exothermic peak becomes largely dominant which suggests the presence of an imperfect P(VDF-TrFE) crystalline phase in nanocomposites at high Au NWs content.

3.3. Nanocomposite bulk conductivity

The electrical conductivity of the insulating P(VDF-TrFE) copolymer is 10^{-12} S m^{-1} at room temperature. The dc electrical conductivity σ_{dc} of the Au NW/P(VDF-TrFE) samples at room temperature is plotted as a function of the Au NW volume fraction (see figure 7). The electrical conductivity increases drastically by 13 orders of magnitude at a very low percolation threshold of 2 vol%. As expected , this value is very low in comparison with the value of 20 vol% obtained for spherical particles [27]. The data points are best fitted by a scaling law according to

$$\sigma = \sigma_0 (p - p_c)^t \qquad (2)$$

with $p_c = 2.2$ vol%, $\sigma_0 = 0.6 \times 10^4$ S m^{-1} and $t = 1.21 \pm 0.27$. The critical exponent value t is smaller than the universal value for three-dimensional percolation systems which is equal to 1.94. From the scaling law, σ_0 is an extrapolation at 100 vol% of Au NWs, which corresponds to the electrical conductivity of Au NWs. The dc conductivity of Au NWs pressed in a sheet

Figure 6. (*a*) Deconvoluted exothermic peaks Tc$_1$ and Tc$_2$ associated with the ferro-para electric transition. (*b*) Enthalpy ratio of ΔH_{C1} to ΔH_{C2} plotted versus Au NW volume fraction.

decrease in crystallinity only at 4 wt% loading [14]. Similar results were obtained by Wang *et al* with 25 wt% of chemically modified copper phthalocyanine (CuPc) oligomers in P(VDF-TrFE) 70-30 copolymer [26].

The geometry of particles and the aspect ratio particularly are the factors providing a higher decrease in crystallinity, except for CNTs [15] which have a nucleating effect and induce a polymer transcrystallinity. To identify precisely the parameter responsible for crystallinity decrease, the effects of Au NWs and spherical particles were compared. Other composites were elaborated with Au particles of diameters 500 nm and 10 μm. The corresponding experimental data points are reported in figure 5. The same linear decrease in crystallinity is observed for each diameter, but the rate of decrease is higher for Au NWs.

The p-f transition temperature is independent of the Au NW volume fraction, which indicates that the fillers are not confined in the P(VDF-TrFE) crystalline phase as expected. The crystallization enthalpy related to Tc$_1$ and Tc$_2$ were calculated from the DSC curves reported in figure 6(*a*). The decrease in enthalpy is found to
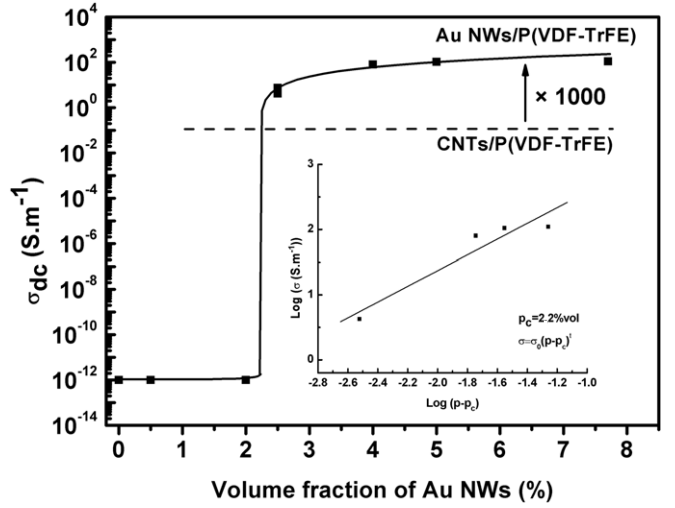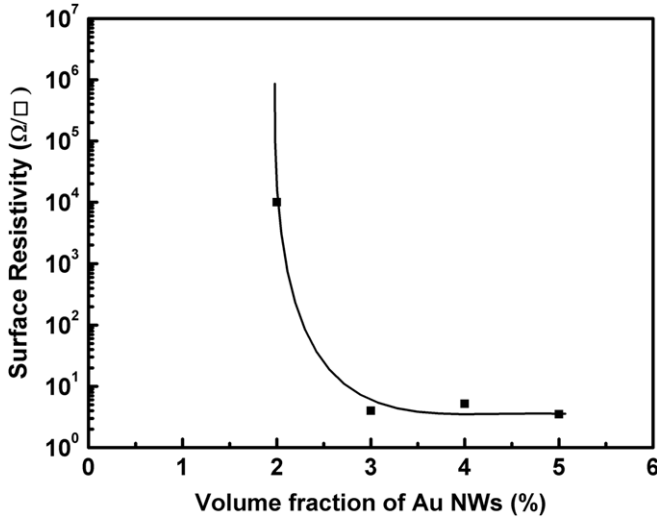
Figure 8. Surface resistivity ρ_s dependence of Au NW volume fraction at $25\,°C$ of sprayed Au NW/P(VDF-TrFE) nanocomposites onto glass substrate.

form was measured to be $1.6 \times 10^4\,S\,m^{-1}$. Hence, σ_0 value is in good agreement with the conductivity of pressed Au NWs.

The Au NWs display a narrow distribution of their aspect ratio centred on an average aspect ratio of $\zeta \approx 225$. According to Balberg and Binenbaum [28], the excluded volume V_{ex} is given in an insulating three-dimensional system containing randomly oriented conductive sticks. This model expresses the critical volume fraction necessary to reach the percolation for a given value of aspect ratio:

$$V_{ex}^{cr} = \frac{L}{r} f_c = 1.6 \pm 0.2. \qquad (3)$$

Assuming the stick is a Au NW, we find a critical volume fraction (f_c) of 0.71 ± 0.08 vol% using (3), a value lower than the experimental one of 2.2 vol%. This difference cannot be explained by the NWs' re-aggregation in the P(VDF-TrFE) matrix or the presence of some bundles of NWs. Figure 2 shows that the Au NW/P(VDF-TrFE) nanocomposites display an acceptable dispersion of NWs, ruling out re-agglomeration. These observations confirm the ability of the metal NWs to be easily dispersed in P(VDF-TrFE) [13]. The curvature of the Au NWs after sonication results in a decrease in their apparent aspect ratio, as shown in the SEM image in figure 1. It is well known in CNT-filled conductive polymer composites that alignment of the filler changes the initial three-dimensional conductive network into a two-dimensional network [29]. Such a decrease in dimensionality could be suggested in Au NW/P(VDF-TrFE) nanocomposites upon an orientation of Au NWs in the P(VDF-TrFE) matrix resulting from the film sample melting process.

Contrary to Ni NWs in P(VDF-TrFE) matrix, Au NWs display the same electrical conductivity as the bulk material [13]. Hence Au NWs do not require the prior surface treatment applied to nickel NWs [13]. Above the percolation threshold, p_c, the electrical conductivity of Au NW/P(VDF-TrFE) nanocomposites is the same as that of Ni NW/P(VDF-TrFE) nanocomposites: $10^2\,S\,m^{-1}$ [13]. According to the preparation

of nanocomposites, this value seems to be the high limit of electrical conductivity using filled metal NWs in P(VDF-TrFE) matrix. This observed conductivity limitation is in good agreement with the values reported for spherical metal nanofillers in homogeneous nanocomposites [27, 30].

3.4. Nanocomposite surface resistivity

The surface resistivity ρ_s was measured on the nanocomposite coatings. Figure 8 shows the surface resistivity as a function of Au NW volume fraction. The resistivity exhibits a percolation threshold around 2 vol%. This result is consistent with the electrical behaviour of the melt-pressed films and rules out the presence of large Au NW aggregates or bundles. At the percolation threshold, the surface resistivity is about $10^4\,\Omega/\square$. Above 3 vol%, ρ_s is constant and is equal to $4\,\Omega/\square$. ρ_s is independent of Au NW volume fraction. This value is more than 1000 times lower than that of the sprayed CNT layer as coating developed by Kaempgen *et al* [31] and 10^6 times lower than that of commercial conductive coatings. Electrically conductive nanocomposite thin films are required for various applications such as electrostatic dissipation or electromagnetic interference shielding.

4. Conclusion

High aspect ratio ($\zeta \sim 225$) Au NWs were successfully prepared by free cyanide electrodeposition into pores of an AAO template. The aspect ratio is preserved after dispersion in a solvent. The intrinsic optical conductivity of Au NWs obtained from valence EELS spectra is in good agreement with their bulk electrical conductivity.

The addition of Au NWs in P(VDF-TrFE) impedes the crystallization process of P(VDF-TrFE) with increasing Au NW volume fraction. The presence of metal filler promotes, in nanocomposites, a less ordered crystalline phase than in pure P(VDF-TrFE) copolymer. The influence of NWs' aspect ratio on the crystallinity decrease was demonstrated.

The Au NW/P(VDF-TrFE) nanocomposites exhibit an electrical percolation threshold at 2.2 vol%. Such a low NW loading results from a homogeneous dispersion of Au NWs in the P(VDF-TrFE) matrix as supported by SEM. A high level of electrical conductivity of $10^2\,S\,m^{-1}$ is reached and is consistent with that of nickel NW/P(VDF-TrFE) nanocomposites. This value is found to be an upper limit for metal NWs or powders as fillers in P(VDF-TrFE). The melt-pressed samples and spray coated samples exhibit the same low percolation threshold. The surface resistivity is about $4\,\Omega/\square$ above the percolation threshold for the conductive coatings.

References

[1] Medalia A I 1986 *Rubber Chem. Technol.* **59** 432
[2] Tang H, Chen X, Tang A and Luo Y 1996 *J. Appl. Polym. Sci.* **59** 383
[3] Untereker D, Lyu S, Schley J, Martinez G and Lohstreter L 2009 *Appl. Mater. Interfaces* **1** 97
[4] Barrau S, Demont P, Peigney A, Laurent C and Lacabanne C 2003 *Macromolecules* **36** 5187
[5] Sandler J K W, Kirk J E, Kinloch I A, Shaffer M S P and Windle A H 2003 *Polymer* **44** 5893
[6] Karttunen M, Ruuskanen P, Pitkanen V and Albers W M 2008 *J. Electron. Mater.* **37** 951
[7] Lee H S, Chou K S and Shih Z W 2005 *Int. J. Adhes. Adhes.* **25** 437
[8] Keshoju K and Sun L 2009 *J. Appl. Phys.* **105** 023515
[9] Miura S, Kiguchi M and Murakoshi K 2007 *Surf. Sci.* **601** 287
[10] Denver H, Heiman T, Martin E, Gupta A and Borca-Tasciuc D A 2009 *J. Appl. Phys.* **106** 064909
[11] Su H L, Ji G B, Tang S L, Chen W, Li Z, Gu B X and Du Y W 2005 *J. Appl. Phys.* **97** 116104
[12] Xu J X, Huang X M, Xie G Z, Fang Y H and Liu D Z 2005 *Mater. Lett.* **59** 981
[13] Lonjon A, Laffont L, Demont P, Dantras and Lacabanne C 2009 *J. Phys. Chem.* C **113** 12002
[14] Vidhate S, Shaito A, Chung J and D'Souza N A 2008 *J. Appl. Polym. Sci.* **112** 254
[15] Wang M, Shi J H, Pramoda K P and Goh S H 2007 *Nanotechnology* **18** 235701
[16] Cebe P and Runt J 2004 *Polymer* **45** 1923
[17] Dillon D, Tenneti, Li K, Ko F, Sics I and Hsiao B 2006 *Polymer* **47** 1678
[18] Clements J, Davies G R and Ward I M 1992 *Polymer* **33** 1623
[19] Schamm S and Zanchi G 2003 *Ultramicroscopy* **96** 559
[20] Cheynet M C and Pantel R 2006 *Micron* **37** 377
[21] Wang Y Y, Zhang H and Dravid V P 1993 *Ultramicroscopy* **52** 523
[22] Walton A S, Allen C S, Critchley K, Gorzny M L, McKendry J E, Brydson R M D, Hickey B J and Evans S D 2007 *Nanotechnology* **18** 065204
[23] Tanaka H, Yukawa H and Nishi T 1988 *Macromolecules* **21** 2463
[24] Moreira R L, Saint-Gregoire P and Latour M 1989 *Phase Transitions* **14** 243
[25] Gregorio R J and Botta M M 1998 *J. Polym. Sci. B: Polym. Phys.* **36** 403
[26] Wang J W, Shen Q D and Yang C Z 2004 *Macromolecules* **37** 2294
[27] Forster R J and Keane L 2003 *J. Electroanal. Chem.* **554** 345
[28] Balberg I and Binenbaum N 1984 *Phys. Rev. Lett.* **52** 1465
[29] Deng H, Zhang R, Bilotti E, Loos J and Peijs T 2009 *J. Appl. Polym. Sci.* **113** 742
[30] Alvarez M P, Poblete V H, Pilleux M E and Fuenzalida V M 2006 *J. Appl. Polym. Sci.* **99** 3005
[31] Kaempgen M, Duesberg G S and Roth S 2005 *Appl. Surf. Sci.* **252** 425